Reynolds number effect on the concentration and preferential orientation of inertial ellipsoids

A. Michel, Boris Arcen

Reynolds number effect on the concentration and preferential orientation of inertial ellipsoids

A. Michel[*] and B. Arcen[†]
Université de Lorraine, CNRS, LEMTA, F-54000 Nancy, France

(Received 7 May 2021; accepted 7 October 2021; published 17 November 2021)

Using direct numerical simulation, the dynamics of ellipsoidal particles in a turbulent channel flow is examined at three values of the friction Reynolds number, $\mathrm{Re}_\tau = 180$, 400, and 550. Once the flow has reached a statistically steady state, the Lagrangian tracking of 300 000 prolate ellipsoids, modeled as point particles, is conducted. A global parameter based on entropy is used to follow the evolution of the particle concentration and reveals that, when expressed in wall units, the duration of the transient period increases with the Reynolds number. Once the particle distribution has reached a statistically stationary state, the distribution is closer to the uniform distribution for high values of Re_τ, with a small influence of the aspect ratio, but a noticeable effect of particle inertia. In the viscous sublayer, where the mean velocity gradient causes Jeffery-like orbiting of the ellipsoids, preferential orientation is affected by Re_τ. The stronger fluctuations of the fluid vorticity occurring at higher Re_τ are responsible for a destabilization of the weakly stable rotation orbits of the spheroids. Spinning particles are more likely to align with the fluid seen vorticity and spend less time aligned with the mean flow, while tumbling particles are more likely to be found out of the mean velocity-gradient plane.

DOI: 10.1103/PhysRevFluids.6.114305

I. INTRODUCTION

The dynamics of particles in turbulent flows is of interest for a wide variety of applications, from the dispersion of plastic particles [1] and plankton [2] in the marine environment to industrial applications such as papermaking [3]. Nonspherical particles can be modeled by spheroids and provide a better understanding of the two-phase flow characteristics than a spherical model, as described by Voth and Soldati [4]. The challenge encountered in predicting the behavior of such flows is linked to the particle shape, whose interaction with the fluid velocity gradient produces a complex orientational dynamics, which in turn modifies particle dispersion. Theoretical formulas allowing the computation of the hydrodynamic actions (force and torque) applied by the flow on ellipsoids at small particle Reynolds numbers (creeping flow regime) were derived by Happel and Brenner [5] and Jeffery [6]. They have been used to explain laboratory results tied to the dynamics of such particles. Krushkal and Gallily [7] observed preferential orientation of Brownian fibers due to the shear magnitude when this parameter is greater than the particle Brownian diffusivity. In a laminar duct flow, Bernstein and Shapiro [8] found preferential orientation of fibers along the mean velocity, but no alignment if the flow is turbulent. Analogous experiments conducted by Newsom and Bruce [9] and Parsheh *et al.* [10] showed that the turbulent intensity of the flow makes the particle orientation uniform. This is closely linked to the ellipsoids' rotation rate, which is modulated

[*]antoine.michel@univ-lorraine.fr
[†]boris.arcen@univ-lorraine.fr

by the particle length and by their orientation relative to the fluid vorticity, as described by Parsa *et al.* [11], Hoseini *et al.* [12], and Sabban *et al.* [13].

As a complement to experiments, numerical simulation has proved to be a convenient tool for studying the dynamics of ellipsoidal particles. In a simple shear, Lundell and Carlsson [14] showed that there is a strong effect of ellipsoid inertia on the rotation orbits predicted by Jeffery [6]. Einarsson *et al.* [15] performed the stability analysis of the rotation equations and concluded that particle inertia increases the stability of the rotation orbits, which results in different preferential orientation. In a turbulent channel flow, the effect produced by particle shape and inertia on various statistics has also been extensively studied. At $\mathrm{Re}_\tau = 125$ (based on the wall shear velocity u_τ and the channel half-width δ), Zhang *et al.* [16] quantified the deposition of fibers modeled as prolate ellipsoids by using point-particle direct numerical simulation (DNS). Marchioli *et al.* [17] worked with a somewhat similar $\mathrm{Re}_\tau = 150$ and provided orientation and velocity statistics. Mortensen *et al.* [18] compared the effect of the particles characteristics on orientation and velocity statistics at $\mathrm{Re}_\tau = 180$ and found a strong effect of the particle shape and inertia on the preferential orientation. This was further studied by Zhao *et al.* [19], who mapped the ellipsoids' rotation mode and found that in the viscous sublayer, the particles' favored rotation plane depends on their aspect ratio and relaxation time. Also at $\mathrm{Re}_\tau = 180$, Challabotla *et al.* [20] and Arcen *et al.* [21] examined preferential orientation in the presence of gravity. The dynamics of ellipsoidal particles in a channel for higher values of Re_τ remains however largely unknown, and few studies have described the influence of this parameter. A scaling of the slip velocity statistics of inertial ellipsoids with the flow Reynolds number was reported by Zhao *et al.* [22]. They worked at $\mathrm{Re}_\tau = 150$, 180, and 300 and suggested possibly different outcomes for higher values of this parameter. At $\mathrm{Re}_\tau = 1000$, Jie *et al.* [23] noticed that preferential orientation of inertialess spheroids is similar to that observed at $\mathrm{Re}_\tau = 180$. Only Ouchene *et al.* [24] conducted simulations with inertial ellipsoids at the much higher $\mathrm{Re}_\tau = 1440$. However, this work is focused on acceleration statistics and the time interval used to compute statistics is short (approximately equal to 300 in wall units), which could introduce a statistical bias in view of the conclusions in Michel and Arcen [25].

To better understand how Re_τ influences the dynamics of inertial spheroids, we perform direct simulations of the turbulent flow in a channel at $\mathrm{Re}_\tau = 180$, 400, and 550. Prolate ellipsoidal particles are then introduced in the flow and their motion is tracked by the Lagrangian method. To ensure that the particle distribution reaches a statistically steady state, the evolution of the particle distribution is tracked by means of an entropy parameter, originally proposed by Picano *et al.* [26], and long-time statistics are computed. The present study focus on the effect of Re_τ on two aspects of the particle dynamics: the particle distribution and the preferential orientation.

II. GOVERNING EQUATIONS

A. Fluid phase

The turbulent flow is described by the continuity and momentum conservation equations for a Newtonian, incompressible, and isothermal fluid:

$$\frac{\partial u_i}{\partial x_i} = 0, \tag{1}$$

$$\frac{\partial u_i}{\partial t} + u_j \frac{\partial u_i}{\partial x_j} = -\frac{1}{\rho_f}\frac{\partial p}{\partial x_i} + \nu \frac{\partial^2 u_i}{\partial x_j \partial x_j}, \tag{2}$$

where u_i is the component of the velocity field in the direction x_i, p the pressure, ρ_f the fluid density, and ν the fluid kinematic viscosity.

B. Lagrangian particle tracking

Particles are modeled as prolate spheroids of aspect ratio $\lambda = a/b > 1$, a and b being the lengths of the semimajor and semiminor axes. Particles are treated as material points; therefore, the coupling

between the fluid and particle phases is modeled and not directly solved. The particle position and orientation are obtained by solving the sets of equations:

$$\frac{\mathrm{d}\mathbf{x}_p}{\mathrm{d}t} = \mathbf{u}_p, \quad m_p \frac{\mathrm{d}\mathbf{u}_p}{\mathrm{d}t} = \mathbf{F}, \tag{3}$$

$$\frac{\mathrm{d}\mathbf{q}_p}{\mathrm{d}t} = \frac{1}{2}\mathbf{q}_p\boldsymbol{\omega}'_p, \quad \mathbf{I}_I \frac{\mathrm{d}\boldsymbol{\omega}'_p}{\mathrm{d}t} + \boldsymbol{\omega}'_p \times (\mathbf{I}_I\boldsymbol{\omega}'_p) = \mathbf{T}', \tag{4}$$

where $\mathbf{x}_p$ and $\mathbf{u}_p$ are the particle position and velocity, $\mathbf{q}_p$ and $\boldsymbol{\omega}'_p$ are the unit quaternion describing the orientation of the particle and particle rotation vector, respectively, $m_p = \rho_p(\frac{4}{3})\pi ab^2$ is the particle mass, ρ_p denotes its density, $\mathbf{I}_I$ is the particle inertia tensor. $\mathbf{F}$ is the fluid force and $\mathbf{T}'$ is the torque acting on the particle. Note that translation equations are solved in the Eulerian frame (x, y, z), while rotation equations are solved in the frame linked to the particle's principal axes (x', y', z'). In this frame, the particle's major axis is aligned with x'.

In the present study, $\mathbf{F}$ is modeled by the formula from Happel and Brenner [5]:

$$\mathbf{F} = \nu\rho_f(\mathbf{A}^{-1}\mathbf{K}\mathbf{A})\mathbf{u}_r, \tag{5}$$

where $\mathbf{u}_r = \tilde{\mathbf{u}} - \mathbf{u}_p$ is the relative velocity between the particle and the fluid, $\tilde{\mathbf{u}} = \mathbf{u}(\mathbf{x}_p, t)$ being the fluid velocity at the particle position. $\mathbf{A}$ is the direction cosine matrix which is used to express vectors and tensors from the Eulerian frame in the particle frame. This matrix is computed knowing the particle orientation, as described in Zhang *et al.* [16]. $\mathbf{K}$ is the translational resistance tensor, which describes the influence of particle shape on its translational motion. It is diagonal in the particle frame (x', y', z'), and for prolate spheroids the components can be found in Gallily and Cohen [27]:

$$K_{x'x'} = \frac{8\pi b(\lambda^2 - 1)}{\left[\ln(\lambda + \sqrt{\lambda^2 - 1})\frac{2\lambda^2 - 1}{\sqrt{\lambda^2 - 1}}\right] - \lambda}, \tag{6}$$

$$K_{y'y'} = \frac{16\pi b(\lambda^2 - 1)}{\left[\ln(\lambda + \sqrt{\lambda^2 - 1})\frac{2\lambda^2 - 3}{\sqrt{\lambda^2 - 1}}\right] + \lambda}, \tag{7}$$

$$K_{z'z'} = K_{y'y'}. \tag{8}$$

In the general case, due to the product $\mathbf{A}^{-1}\mathbf{K}\mathbf{A}$, $\mathbf{F}$ can be decomposed as $\mathbf{F} = \mathbf{F}_D + \mathbf{F}_L$, where $\mathbf{F}_D$ is the drag force, the component of $\mathbf{F}$ collinear to $\mathbf{u}_r$, while $\mathbf{F}_L$ is the lift force, the component of $\mathbf{F}$ orthogonal to $\mathbf{u}_r$. This lift force appears purely as a consequence of particle anisotropy and orientation and it is not related to the shear-induced lift, for which an expression was recently proposed by Cui *et al.* [28].

With $\mathbf{F}$ known, the particle relaxation time can be obtained. It is the characteristic time required for a particle to adjust to a change in the flow characteristics. This time is not unique and several definitions are summed up by Siewert *et al.* [29]. We use the definition from Shapiro and Goldenberg [30], obtained by averaging $\mathbf{K}$ over an isotropic orientation distribution:

$$\tau_p = \frac{2\rho_p b^2}{9\rho_f \nu} \frac{\ln(\lambda + \sqrt{\lambda^2 - 1})}{\sqrt{\lambda^2 - 1}}. \tag{9}$$

When expressed in wall units (using u_τ and ν), this is the particle Stokes number: the ratio of the particle relaxation time to the viscous timescale of the flow (ν/u_τ^2).

TABLE I. Number of mesh points, grid spacings, and temporal increment.

Re_b	Re_τ	N_x	N_y	N_z	Δ_x^+	Δ_y^+	Δ_z^+	Δt^+
2820	179	288	128	160	7.85	0.98−4.44	4.67	0.11
7100	396	320	256	300	7.85	1.08−4.94	5.45	0.09
10050	543	450	352	400	7.68	1.08−4.94	5.62	0.08

The torque is modeled with the formula from Jeffery [6]:

$$\mathbf{T}' = \frac{16\pi\mu ab^2}{3}\begin{pmatrix} \dfrac{1}{\beta_0}[(\Omega'_{zy}-\omega'_{px})] \\ \dfrac{1}{\beta_0+\lambda^2\alpha_0}[(1-\lambda^2)S'_{xz}+(1+\lambda^2)(\Omega'_{xz}-\omega'_{py})] \\ \dfrac{1}{\lambda^2\alpha_0+\beta_0}[(\lambda^2-1)S'_{yx}+(\lambda^2+1)(\Omega'_{yx}-\omega'_{pz})] \end{pmatrix}, \tag{10}$$

where μ is the fluid dynamic viscosity, ω'_{px}, ω'_{py}, and ω'_{pz} are the components of the particle angular velocity. $S'_{ij} = \frac{1}{2}(\partial u'_i/\partial x'_j + \partial u'_j/\partial x'_i)$ is the fluid rate-of-strain tensor and $\Omega'_{ij} = \frac{1}{2}(\partial u'_i/\partial x'_j - \partial u'_j/\partial x'_i)$ is the rate-of-rotation tensor at the particle location. The components of both tensors are given with respect to the particle frame (x', y', z'). The coefficients α_0 and β_0 are provided by Oberbeck [31] as integrals and their explicit expressions are given by Gallily and Cohen [27].

These formulas are valid if the particle Reynolds number $\mathrm{Re}_p = d_{eq}\|\mathbf{u}_r\|/\nu \ll 1$, where $d_{eq} = 2b\sqrt[3]{\lambda}$ is the diameter of the volume equivalent sphere. In this study, Re_p is typically less than 1 and the formulas from Happel and Brenner [5] and Jeffery [6] are valid within this range of Re_p.

III. SIMULATION SETUP

The turbulent flow in a channel of width 2δ is computed at three different Reynolds numbers by a finite-difference DNS solver. More details on this solver can be found in Michel and Arcen [25]. Periodic boundary conditions are applied in the x and z directions (statistically homogeneous directions) and a no-slip–no-penetration condition is enforced at $y = \pm\delta$. Similarly to the finite-difference code used by Vreman and Kuerten [32], the spatial derivatives appearing in Eqs. (1) and (2) are approximated using fourth-order schemes in the streamwise and spanwise directions, while second-order schemes are used in the wall-normal direction. The time advancement is performed by a fully explicit third-order low-storage Runge-Kutta scheme [33] and the time step is obtained by fixing a constant Courant-Friedrichs-Lewy number of 0.5. At each Runge-Kutta stage, the pressure-velocity coupling problem is solved using the pressure-correction method proposed by Timmermans *et al.* [34].

The mean flow is directed along x and the flow rate is kept constant. In our simulations, the bulk Reynolds number $\mathrm{Re}_b = U_b\delta/\nu$, based on the mean bulk velocity U_b, is thus directly specified. In the present study, three target Reynolds numbers, based on the wall-shear velocity, are considered: $\mathrm{Re}_\tau = 180$, 400, and 550. A preliminary study of the flow statistics has shown very good agreement with the statistics provided by Vreman and Kuerten [32], Moser *et al.* [35], and Lee and Moser [36], respectively. The relative error on the mean and rms velocity and vorticity profiles did not exceed 1.5%. The input parameters Re_b as well as the number of mesh points, grid spacings, and averaged time step are summed up in Table I.

Particles are modeled as prolate spheroids. Three aspect ratios $\lambda = 1$, 3, and 10 are investigated as well as three relaxation times in wall units $\tau_p^+ = 1$, 5, and 30. Particle geometry was chosen so that the volume equivalent sphere diameter remains constant and a^+ remains of the same order of magnitude as Kolmogorov's length scale. The particle parameters are provided in Table II. To focus on the effect of turbulence on the particle dynamics, the particle-fluid coupling is one way:

TABLE II. Characteristics of prolate spheroids. The volume equivalent sphere diameter is constant and equal to $d_{eq}^+ = 1$.

			ρ_p/ρ_f		
λ	a^+	b^+	$\tau_p^+ = 1$	$\tau_p^+ = 5$	$\tau_p^+ = 30$
1	0.50	0.50	18	90	540
3	1.04	0.35	20	100	601
10	2.32	0.23	27.8	139	833

the effect of the particle on the fluid is supposed negligible as well as the interparticle interactions. Periodic boundaries are applied in the streamwise and spanwise directions. Wall-particle collisions are treated as elastic when the distance between the particle center of mass and the wall is smaller than $d_{eq}/2$. The equations governing the ellipsoidal translational and rotational motions are solved with the same third-order low-storage Runge-Kutta scheme as used in the fluid solver. The fluid velocity and velocity gradient necessary to compute the hydrodynamic actions on each particle are interpolated at the particle's position using a tricubic Hermite interpolation and a trilinear interpolation, respectively.

300 000 prolate spheroids are seeded uniformly in the turbulent flow field. The particle translational and rotational velocities are initially equal to that of the fluid at their position, while their orientation is randomized. Particles are tracked for 50 000 viscous time units and the instantaneous metrics of the particles are collected every 200 iterations over the interval $t^+ \in [30\,000, 50\,000]$ to produce statistics. For all particles sets, the distribution in the channel has reached a statistically steady state before $t^+ = 30\,000$ and consequently no bias is introduced in the statistics.

IV. RESULTS AND DISCUSSION

A. Temporal evolution of the particle distribution

One of the well-known characteristics of particle flows is the gradual accumulation of the particles at the wall; thus we start by investigating the temporal evolution of the particle distribution. The distribution can be more easily understood by means of the parameter S proposed by Picano *et al.* [26], based on the entropy defined by Shannon [37]. At a given time t^+, $S(t^+) = -\sum_{i=1}^{M} p_i(t^+) \ln[p_i(t^+)]/\ln(N_T)$, where $p_i(t^+) = N_i(t^+)/N_T$, M is the number of wall-parallel slabs used to uniformly split the domain, N_T is the total number of particles tracked, and $N_i(t^+)$ is the number of particles in the ith slab at a given t^+. The value of the parameter S is 1 if the particles are uniformly distributed and 0 if they are all in the same subvolume. Knowing that particles tend to accumulate in the viscous sublayer, this parameter offers a good overview of the particle distribution. The present results have been computed with $M = 100$ for each Re_τ.

The evolution of the entropy parameter is presented in Figs. 1(a)–1(c). The constant unit-valued entropy attests that the distribution of $\tau_p^+ = 1$ particles remains uniform at all Re_τ. In contrast, a clear effect of the Reynolds number is visible for inertial particles and the evolution of the particle distribution is affected in two ways. First, the time required for the distribution to reach steady state increases as Re_τ increases. This is very pronounced for $\tau_p^+ = 30$ particles, which require about twice as much time to reach steady state at $\mathrm{Re}_\tau = 550$ compared to $\mathrm{Re}_\tau = 180$, and similarly for all the aspect ratios. For $\tau_p^+ = 5$ particles, the increase is less significant for spheres and $\lambda = 10$, but remains visible for $\lambda = 3$ ellipsoids. These ($\lambda = 3$) are the particles whose entropy reaches the lowest value; therefore, many particles have to reach the sublayer for S to stabilize. Due to the stronger velocity fluctuations, this likely takes a longer time at higher Reynolds number. Another visible effect is that a high value of Re_τ increases the steady-state value of the entropy parameter, whatever the particle inertia and aspect ratio. The increase of the entropy indicates that the particle

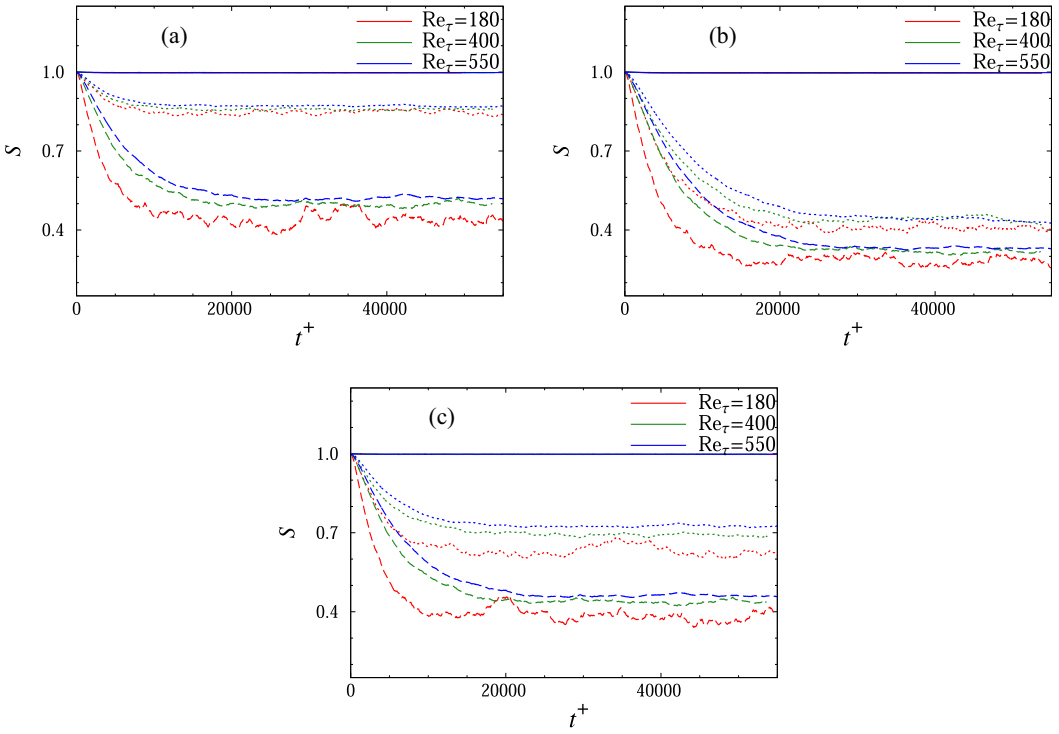

FIG. 1. Temporal evolution of the entropy parameter S for ellipsoids of different aspect ratios (a) $\lambda = 1$, (b) $\lambda = 3$, and (c) $\lambda = 10$ for relaxation times $\tau_p^+ = 1$ (solid lines), $\tau_p^+ = 5$ (dotted lines), and $\tau_p^+ = 30$ (dashed lines).

distribution is closer to uniform. During the steady state, particle wall-normal motion is controlled by the cycle of turbulent events (sweeps and ejections) generated by coherent streamwise vortices [38]. These fluctuations are stronger at higher Re_τ, and more particles are likely to be ejected out of the sublayer because of the intensity of these events. A quadrant analysis of the fluid velocity sampled at the particle position (not shown here) confirmed that the particle fraction in sweeps and ejections events remains independent of Re_τ and that only the intensity of the events increases with the flow Reynolds number.

The influence of the flow Reynolds number on the steady-state concentration is now examined. In the ith slab used to compute entropy, the concentration is obtained by $C_i = N_i/V_i$, where C_i is the concentration, N_i the number of particles, and V_i the slab volume. It is normalized by $C_0 = N_T/(L_x L_y L_z)$, the average concentration in the channel. The concentration profiles averaged over the range $t^+ \in [30\,000, 50\,000]$ are presented in Figs. 2(a)–2(c) as a function of $y^* = y/\delta$. As noted from S, the distribution of $\tau_p^+ = 1$ spheres and ellipsoids is nearly uniform, with a slight increase in the near-wall region. This is due to the small (but nonzero) value of the relaxation time, which is sufficient to observe an effect of inertia. Note that the nonuniformity of the concentration profile was barely visible on the entropy plot in Figs. 1(a)–1(c), as the value of S remains near 1. As the particle relaxation time increases, the near-wall concentration increases while the core concentration decreases. This is consistent with the decrease of the entropy parameter previously noted. Figure 2 also shows that there is a strong effect of the particle shape on the concentration profile, especially for $\tau_p^+ = 5$, for which the concentration of ellipsoids is higher than spheres near the wall. This increased segregation has been attributed to the additional lift force induced by the coupled effect of particle shape and orientation [25]. Also, this is less pronounced for $\tau_p^+ = 30$ and was anticipated from the value of S.

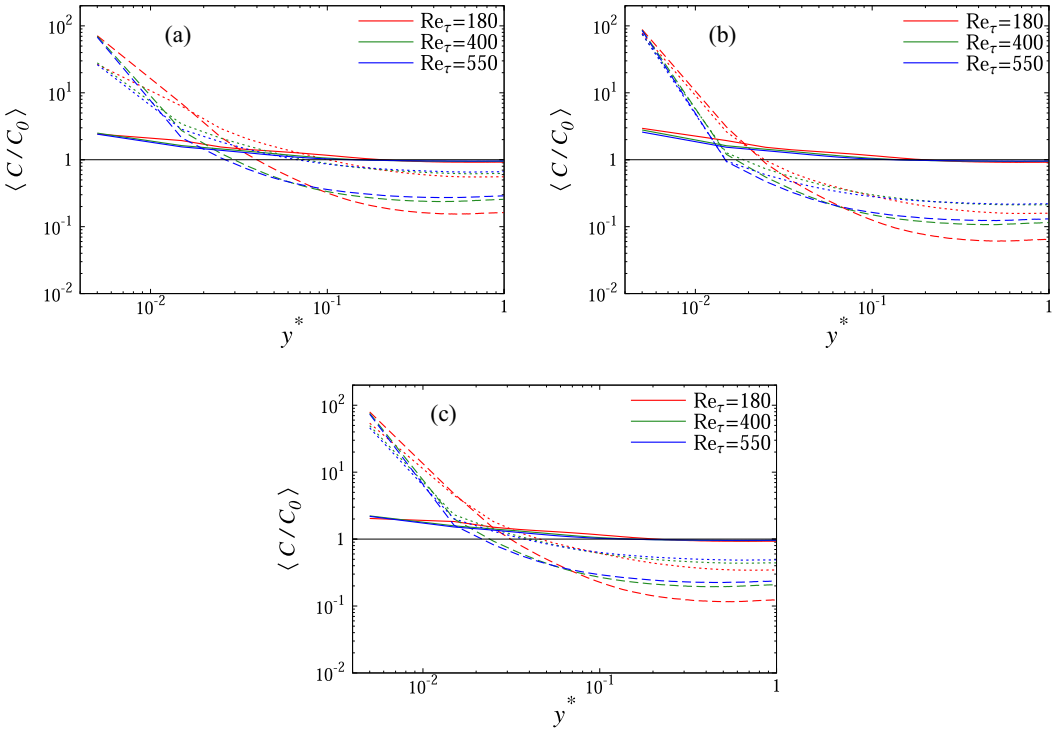

FIG. 2. Average concentration profile as a function of y^* for ellipsoids of different aspect ratios (a) $\lambda = 1$, (b) $\lambda = 3$, and (c) $\lambda = 10$ for relaxation times $\tau_p^+ = 1$ (solid lines), $\tau_p^+ = 5$ (dotted lines), and $\tau_p^+ = 30$ (dashed lines).

Very close to the wall, for a given aspect ratio and relaxation time, the concentration is unaffected by the Reynolds number. While moving away from the wall, an effect of the Reynolds number is visible for $\tau_p^+ = 5$ and 30. The concentration profile decreases more quickly for higher values of Re_τ. A parallel can be drawn between this observation and the results reported by Bernardini [39], who noticed that in wall units, the concentration profile of spheres scaled with Re_τ in the viscous sublayer. When expressed in bulk units, the size of this region decreases with Re_τ and the profile exhibits a more negative slope. For a given τ_p^+, this results in a more important concentration for small values of Re_τ up to $y^* \approx 0.1$. From this location, the concentration is higher for higher Re_τ, and this explains the more important value of the entropy observed in Figs. 1(a)–1(c). We conclude by remarking that the conclusions drawn for ellipsoids are in qualitative agreement with the ones reported for spheres by Bernardini [39]. Nonetheless, significant quantitative differences can be observed due to the particles' shape, which affect the dispersion through their orientational dynamics.

Finally, it should be noted that for weakly inertial fibers, a slight increase of the near-wall concentration was measured experimentally by Alipour *et al.* [40] and numerically by Do-Quang *et al.* [41] using particle-resolved simulations. This trend is similar to what we observe for $\lambda = 10$ and $\tau_p^+ = 1$ ellipsoids. Consequently, one-way coupled point-particle simulation seems appropriate to estimate the concentration of such particles. For more inertial particles, the high near-wall concentration noted in the present study should be taken with care since the collisions between particles as well as the influence of the dispersed phase on the carrier flow were not accounted for. These two mechanisms are expected to attenuate the near-wall accumulation, as it was observed by Costa *et al.* [42] for spherical particles.

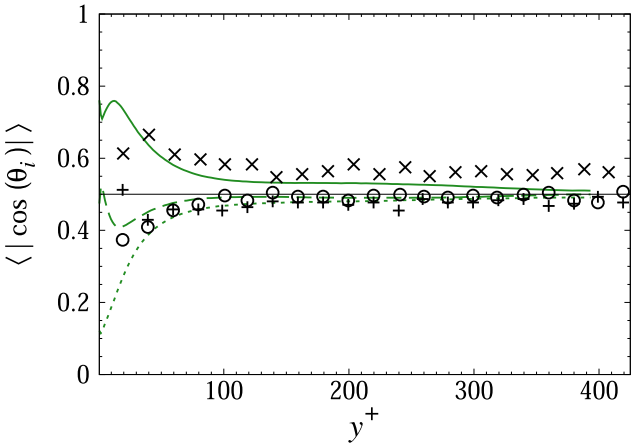

FIG. 3. Comparison of the average absolute direction cosine obtained from DNS at $\mathrm{Re}_\tau = 400$ for $\tau_p^+ = 1$ and $\lambda = 10$ with experimental data provided by Shaik *et al.* [43] at $\mathrm{Re}_\tau = 435$. Present study: $\langle|\cos(\theta_x)|\rangle$ (solid line), $\langle|\cos(\theta_y)|\rangle$ (dotted line), and $\langle|\cos(\theta_z)|\rangle$ (dashed line). Shaik *et al.* [43]: $\langle|\cos(\theta_x)|\rangle$ ($\times$), $\langle|\cos(\theta_y)|\rangle$ ($\bigcirc$), and $\langle|\cos(\theta_z)|\rangle$ ($+$).

B. Particle orientation

The absolute value of the direction cosine $|\cos(\theta_i)|$ provides information on the orientation of the particle's major axis relative to the Eulerian frame. In the three-dimensional case, a value close to 1 indicates a strong alignment of the particle with the ith axis of the Eulerian frame, while a value near 0 reveals an orientation orthogonal to this axis. A value around 0.5 indicates a uniform orientation. We first examine the agreement between our DNS computed orientation and experimental measurements and then the effect of the flow Reynolds number will be studied.

The DNS results at $\mathrm{Re}_\tau = 400$ for $\lambda = 10$ and $\tau_p^+ = 1$ ellipsoids are compared with the mean orientation of weakly inertial and long fibers ($\lambda = 30$ and $\tau_p^+ = 0.22$) measured by Shaik *et al.* [43] at $\mathrm{Re}_\tau = 435$ in Fig. 3. They already conducted a comparison with existing point-particle and finite-size DNS data; nevertheless, these data were obtained at a much lower Re_τ. From Fig. 3, quantitative differences are noticed for $y^+ < 40$ but there is good qualitative agreement between the DNS and experiment. We notice a maximum of $\langle|\cos(\theta_x)|\rangle$ and a minimum for $\langle|\cos(\theta_z)|\rangle$ in both studies, but these are shifted about 30 viscous units towards the channel center in the experiment. This is about the same as the fiber length used by Shaik *et al.* [43] and it indicates a likely consequence of particle-wall interaction. In the channel core, there is very good agreement between the DNS and experimental data, and only the DNS results for $\langle|\cos(\theta_x)|\rangle$ are slightly lower than the experimental data.

To examine the influence of the Reynolds number on the orientation, the three components of the averaged direction cosines are plotted in Fig. 4 for the three values of Re_τ considered. The most obvious effect of increasing Re_τ is that it decreases the fraction of the channel over which preferential orientation occurs. Bernstein and Shapiro [8] showed that preferential orientation is a consequence of the organizing effect of the mean velocity gradient. Preferential orientation was further studied by Zhao and Andersson [44], who showed that inertialess prolate spheroids preferentially align with the direction of the maximum Lagrangian stretching. They emphasized that in the viscous sublayer, the strongest Lagrangian stretching is oriented in the streamwise direction, and this corresponds to the preferential alignment of weakly inertial particles in this region. As Re_τ increases, the size of the viscous sublayer, expressed in terms of the channel half width (δ), diminishes and preferential orientation is visible in a narrower region of the channel. Particles located farther from the wall exhibit a lower degree of organization, because the effect of the mean

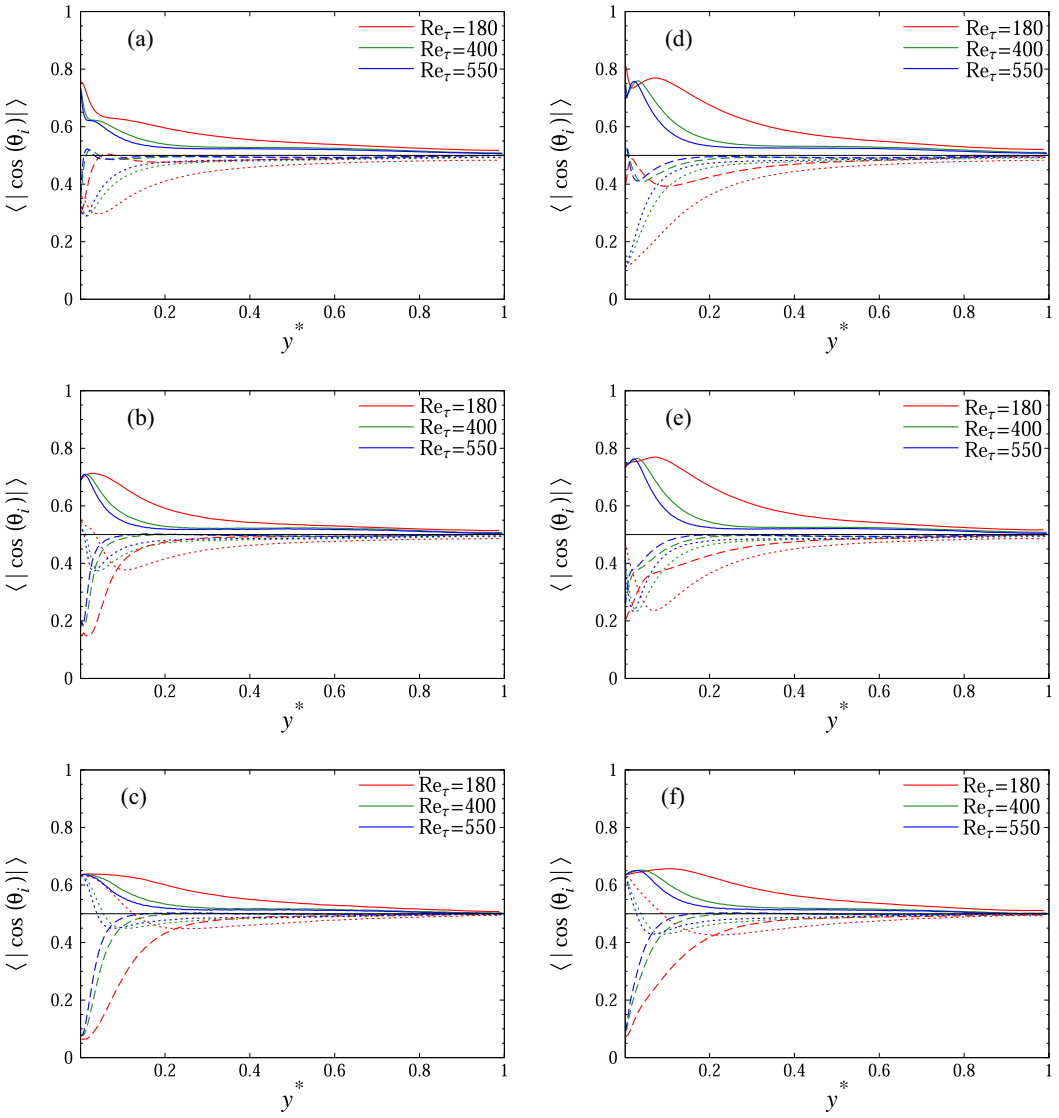

FIG. 4. Average absolute direction cosine for spheroids of different aspect ratios (a)–(c) $\lambda = 3$ and (d)–(f) $\lambda = 10$ and relaxation times (a) and (d) $\tau_p^+ = 1$, (b) and (e) $\tau_p^+ = 5$, and (c) and (f) $\tau_p^+ = 30$: $|\cos(\theta_x)|$ (solid lines), $|\cos(\theta_y)|$ (dotted lines), and $|\cos(\theta_z)|$ (dashed lines).

gradient is overcome by the randomizing effect of the vorticity fluctuations. In the channel core, particle orientation is almost uniform, independently of Re_τ.

Near the wall, preferential orientation stems from the periodic rotation of the particles induced by the mean velocity gradient. This mechanism depends strongly on particle shape and inertia. For instance, Zhao *et al.* [19] showed that inertialess particles of high λ spin in the (x, z) plane. This is similarly observed for $\tau_p^+ = 1$ particles, for which low values of $\langle|\cos(\theta_y)|\rangle$ at the wall in Fig. 4(d) confirm that the particle's major axis lies in the (x, z) plane. To identify the rotation mode, we present in Figs. 5(a) and 5(b) the probability density function (PDF) of $|\cos(\beta)|$ in the slab $1 < y^+ < 2$, β being the angle between the particle's major axis and its rotation vector. Figure 5(b) shows that the PDF of $|\cos(\beta)|$ has a peak near 1 for $\lambda = 10$ and $\tau_p^+ = 1$. This implies alignment

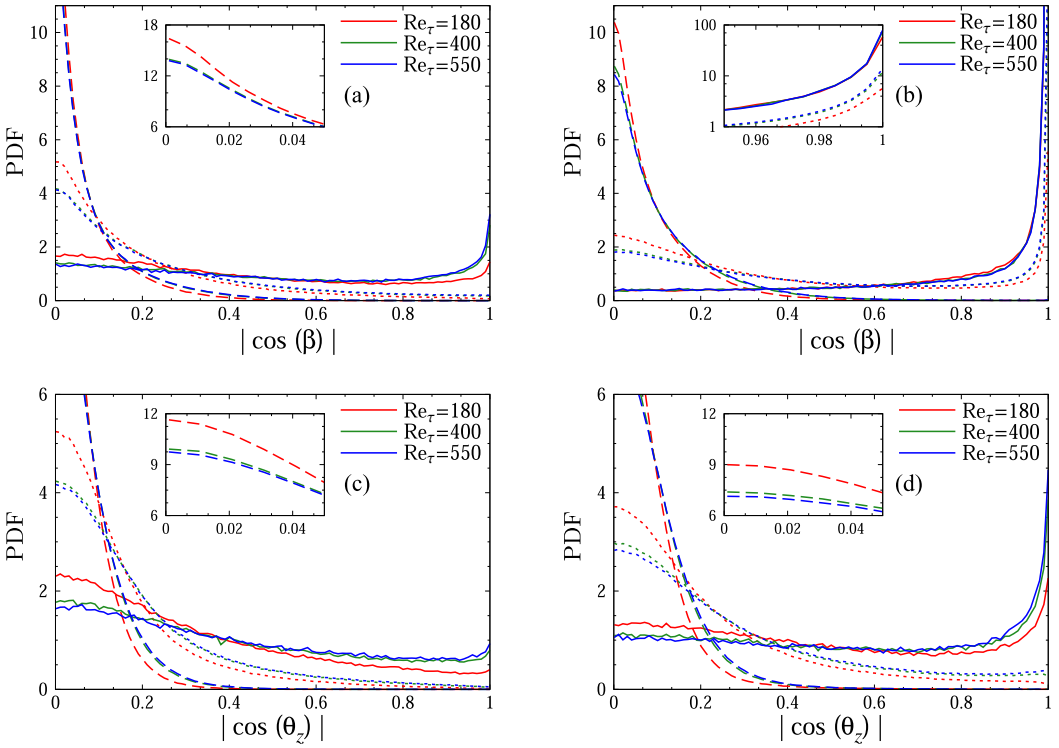

FIG. 5. PDF in the slab $1 < y^+ < 2$ of the absolute direction cosine of β, the angle between the particle major axis and its angular velocity, and of the absolute direction cosine of θ_z, the angle between the particle major axis and spanwise direction, for (a) and (c) $\lambda = 3$ and (b) and (d) $\lambda = 10$ and relaxation times $\tau_p^+ = 1$ (solid lines), $\tau_p^+ = 5$ (dotted lines), and $\tau_p^+ = 30$ (dashed lines).

of the particle's major axis with their rotation vector, which corresponds to spinning. In addition, these particles spend long periods of time nearly aligned with the mean flow since high values of $\langle|\cos(\theta_x)|\rangle$ are noticed. A somewhat similar behavior is observed for $\lambda = 3$ and $\tau_p^+ = 1$, as well as for $\lambda = 10$ and $\tau_p^+ = 5$, but a significant part of these particles is also aligned with y. In comparison, $\tau_p^+ = 30$ as well as $\tau_p^+ = 5$ and $\lambda = 3$ ellipsoids orient in the plane (x, y), since values of $\langle|\cos(\theta_z)|\rangle$ near 0 are noted in Figs. 4(b), 4(c), and 4(f). From the peak near zero in the PDF of β [Figs. 5(a) and 5(b)], we notice that these particles rotate with their major axis orthogonal to the rotation vector. This rotation mode is referred to as tumbling. We also remark that the values of $\langle|\cos(\theta_x)|\rangle$ and $\langle|\cos(\theta_y)|\rangle$ are both equal to 0.634 at the wall for $\tau_p^+ = 30$. This particular value can be compared to the mean absolute direction cosine obtained for a particle rotating with a constant angular velocity in the plane (x, y). For such a uniform circular motion, the mean absolute direction cosines $\langle|\cos(\theta_x)|\rangle$ and $\langle|\cos(\theta_y)|\rangle$ are equal to $(1/T)\int_0^T |\cos[\theta_x(t)]|dt$, with $\theta_x(t) = \omega_{pz}\, t$ and $T = 2\pi/\omega_{pz}$ the rotation period. The exact solution of this integral is $2/\pi \approx 0.636$; this value is nearly identical to the one provided by our computations. Therefore, this implies that $\tau_p^+ = 30$ particles rotate with a nearly constant angular velocity in the near-wall region. This rotation mode appears due to the stabilizing effect of the mean velocity gradient.

Comparison of the near-wall orientation results reveals a notable influence of Re_τ. Figure 4 shows that the value of $\langle|\cos(\theta_z)|\rangle$ at the wall increases with Re_τ for all the relaxation times. This indicates a decrease of preferential orientation for tumbling particles, which are more likely to be found out of the (x, y) plane, while spinning particles spend less time nearly aligned with the mean flow. We can observe these trends by means of the PDF of $|\cos(\theta_z)|$. From Figs. 5(c) and 5(d) we note that the

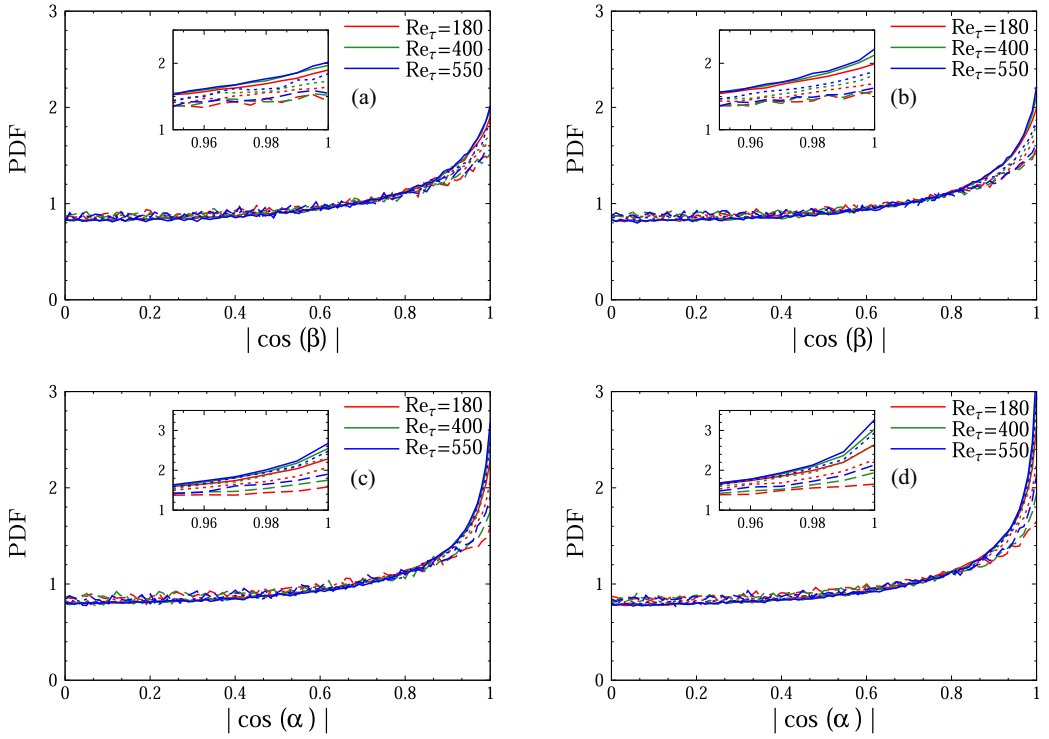

FIG. 6. PDF in the channel core of the absolute direction cosine of β, the angle between the particle major axis and its angular velocity, and of the absolute direction cosine of α, the angle between the particle major axis and the fluid vorticity, for (a) and (c) $\lambda = 3$ and (b) and (d) $\lambda = 10$ and relaxation times $\tau_p^+ = 1$ (solid lines), $\tau_p^+ = 5$ (dotted lines), and $\tau_p^+ = 30$ (dashed lines). The channel core is defined as $170 < y^+ < 180$ for $\mathrm{Re}_\tau = 180$, $380 < y^+ < 400$ for $\mathrm{Re}_\tau = 400$, and $520 < y^+ < 550$ for $\mathrm{Re}_\tau = 550$.

PDF of $|\cos(\theta_z)|$ has a peak near 0 for tumbling particles. The peak magnitude is less important for higher Re_τ; this clearly shows that more particles are found outside the (x, y) plane. Comparatively, spinning particles ($\lambda = 10$ and $\tau_p^+ = 1$) have a stronger alignment with the spanwise direction. Higher Re_τ induces larger values of the PDF of $|\cos(\theta_z)|$ near 1, hence indicating a more pronounced alignment with z. This trend is consistent with the decrease of the streamwise orientation observed in Fig. 4. A similar influence of Re_τ is observed on particles whose rotation cannot be characterized as pure tumbling or pure spinning ($\tau_p^+ = 5$ and $\lambda = 10$, and $\tau_p^+ = 1$ and $\lambda = 3$). For these ellipsoids, Figs. 5(a) and 5(b) indicate that higher Reynolds number enhances spinning and reduces tumbling. In addition, preferential particle alignment shifts towards the spanwise direction. We can link these results to the stability analysis from Einarsson *et al.* [15], who showed that prolate spheroids rotation orbits are weakly stable. Fluctuations of the vorticity field increase with Re_τ [45], and these are sufficient to destabilize the ellipsoids rotation orbits. This results in a substantial modification of the near-wall preferential orientation, regardless of particle inertia.

In the channel core, the effect of the mean velocity gradient is dominated by the vorticity fluctuations and particle orientation is nearly isotropic. The PDF of β shown in Figs. 6(a) and 6(b) reveals that particles in this region favor spinning regardless of their characteristics. The particle aspect ratio has a weak influence on the PDF of β, but increasing the relaxation time decreases alignment between the particle's major axis and its angular velocity vector. To highlight the link between particle dynamics and the vorticity, we also present the PDF of α, the angle between the major axis and the fluid seen vorticity. Figures 6(c) and 6(d) show the PDF of α and reveal that

particle alignment with the fluid seen vorticity occurs in the channel core, whatever λ and τ_p^+. This phenomenon is similar to that noted by Pumir and Wilkinson [46] for tracer spheroids in homogeneous isotropic turbulence. Increasing Re_τ strengthens this preferential alignment as well as the spinning rotation mode for all particles. It appears that the isotropiclike turbulence in this region causes universal rotational dynamics of the ellipsoids.

V. CONCLUSION

The effect of the flow Reynolds number on the concentration and orientation of inertial ellipsoidal particles has been investigated by means of a DNS coupled with a Lagrangian particle tracking. The turbulent flow was simulated at three different Reynolds numbers $\mathrm{Re}_\tau = 180$, 400, and 550. Particles were modeled as ellipsoids with aspect ratios $\lambda = 1$, 3, and 10 and relaxation times $\tau_p^+ = 1$, 5, and 30 and treated as material points under one-way coupling assumption. First, the dynamics of the particle distribution was examined using an entropy parameter S. The evolution of this parameter indicates that increasing the Reynolds number increases the duration of the transient when expressed in wall units, and this effect is stronger when the particle steady-state distribution is highly nonuniform. For particles of the same characteristics, the steady-state concentration increases in the channel core as Re_τ increases, while the concentration in the buffer region decreases. We believe that this is a consequence of the stronger intensity of the turbulent events experienced by the particles at higher Re_τ, which eject particles deeper into the channel core. No changes were observed in the near-wall concentration. While quantitative differences were observed between the different particle sets, the overall picture remains independent of the particle shape. Following this, the effect of the flow Reynolds number on the particle orientation was described by the average absolute direction cosines. Particle orientation in the channel core is nearly uniform and preferential orientation occurs in the viscous sublayer, regardless of the flow Reynolds number. When compared to the channel width, the size of the viscous sublayer decreases when Re_τ increases and causes preferential orientation to be restricted to a narrower region of the channel. In this region, Jeffery-like orbiting of the particles, caused by the mean velocity gradient, induces preferential orientation, which is modified by Re_τ. For low inertia particles, which favor rotation in the (x, z) plane, alignment with the mean flow vorticity increases. For more inertial particles, which tumble in the (x, y) plane, the vorticity fluctuations cause a drift of the particle orbits out of this plane. The increase of the vorticity fluctuations taking place at higher Re_τ is sufficient to reduce preferential orientation caused by the weakly stable Jeffery orbit in the near-wall region. In the channel core, particle orientation is isotropic, but alignment with the fluid seen vorticity occurs regardless of particle characteristics. Finally, increasing Re_τ promotes spinning rotation mode while decreasing tumbling.

The trends observed in this study indicate that increasing the value of Re_τ homogenizes the particle distribution and promotes spinning of ellipsoids in the channel core, whatever τ_p^+. In the viscous sublayer this rotation mode is also enhanced for particles of moderate inertia. At higher values of the Reynolds number, these effects are expected to be more pronounced.

ACKNOWLEDGMENT

High Performance Computing resources were partially supplied by the EXPLOR centre hosted by the University of Lorraine.

[1] L. G. A. Barboza and B. C. G. Gimenez, Microplastics in the marine environment: Current trends and future perspectives, Mar. Pollut. Bull. **97**, 5 (2015).

[2] J. S. Font-Muñoz, R. Jeanneret, I. Tuval, and G. Basterretxea, Method for the determination of preferential orientation of marine particles from laser diffraction measurements, Opt. Express **28**, 14085 (2020).

[3] F. Lundell, L. D. Söderberg, and P. H. Alfredsson, Fluid mechanics of papermaking, Annu. Rev. Fluid Mech. **43**, 195 (2011).
[4] G. A. Voth and A. Soldati, Anisotropic particles in turbulence, Annu. Rev. Fluid Mech. **49**, 249 (2017).
[5] J. Happel and H. Brenner, *Low Reynolds Number Hydrodynamics* (Prentice-Hall, Englewood Cliffs, 1965).
[6] G. B. Jeffery, The motion of ellipsoidal particles immersed in a viscous fluid, Proc. R. Soc. London Ser. A **102**, 161 (1922).
[7] E. Krushkal and I. Gallily, On the orientation distribution function of nonspherical aerosol particles in a general shear flow. I: The laminar case, J. Colloid Interface Sci. **99**, 141 (1984).
[8] O. Bernstein and M. Shapiro, Direct determination of the orientation distribution function of cylindrical particles immersed in laminar and turbulent shear flows, J. Aerosol Sci. **25**, 113 (1994).
[9] R. K. Newsom and C. W. Bruce, Orientational properties of fibrous aerosols in atmospheric turbulence, J. Aerosol Sci. **29**, 773 (1998).
[10] M. Parsheh, M. L. Brown, and C. K. Aidun, On the orientation of stiff fibres suspended in turbulent flow in a planar contraction, J. Fluid Mech. **545**, 245 (2005).
[11] S. Parsa, E. Calzavarini, F. Toschi, and G. A. Voth, Rotation Rate of Rods in Turbulent Fluid Flow, Phys. Rev. Lett. **109**, 134501 (2012).
[12] A. A. Hoseini, F. Lundell, and H. I. Andersson, Finite-length effects on dynamical behavior of rod-like particles in wall-bounded turbulent flow, Int. J. Multiphase Flow **76**, 13 (2015).
[13] L. Sabban, A. Cohen, and R. van Hout, Temporally resolved measurements of heavy, rigid fibre translation and rotation in nearly homogeneous isotropic turbulence, J. Fluid Mech. **814**, 42 (2017).
[14] F. Lundell and A. Carlsson, Heavy ellipsoids in creeping shear flow: Transitions of the particle rotation rate and orbit shape, Phys. Rev. E **81**, 016323 (2010).
[15] J. Einarsson, F. Candelier, F. Lundell, J. R. Angilella, and B. Mehlig, Rotation of a spheroid in a simple shear at small Reynolds number, Phys. Fluids **27**, 063301 (2015).
[16] H. Zhang, G. Ahmadi, F.-G. Fan, and J. B. McLaughlin, Ellipsoidal particles transport and deposition in turbulent channel flows, Int. J. Multiphase Flow **27**, 971 (2001).
[17] C. Marchioli, M. Fantoni, and A. Soldati, Orientation, distribution, and deposition of elongated, inertial fibers in turbulent channel flow, Phys. Fluids **22**, 033301 (2010).
[18] P. H. Mortensen, H. I. Andersson, J. J. J. Gillissen, and B. J. Boersma, Dynamics of prolate ellipsoidal particles in a turbulent channel flow, Phys. Fluids **20**, 093302 (2008).
[19] L. Zhao, N. R. Challabotla, H. I. Andersson, and E. A. Variano, Mapping spheroid rotation modes in turbulent channel flow: Effects of shear, turbulence and particle inertia, J. Fluid Mech. **876**, 19 (2019).
[20] N. R. Challabotla, L. Zhao, and H. I. Andersson, On fiber behavior in turbulent vertical channel flow, Chem. Eng. Sci. **153**, 75 (2016).
[21] B. Arcen, R. Ouchene, M. Khalij, and A. Tanière, Prolate spheroidal particles' behavior in a vertical wall-bounded turbulent flow, Phys. Fluids **29**, 093301 (2017).
[22] L. Zhao, C. Marchioli, and H. I. Andersson, Slip velocity of rigid fibers in turbulent channel flow, Phys. Fluids **26**, 063302 (2014).
[23] Y. Jie, C. Xu, J. R. Dawson, H. I. Andersson, and L. Zhao, Influence of the quiescent core on tracer spheroidal particle dynamics in turbulent channel flow, J. Turbul. **20**, 424 (2019).
[24] R. Ouchene, J. I. Polanco, I. Vinkovic, and S. Simoëns, Acceleration statistics of prolate spheroidal particles in turbulent channel flow, J. Turbul. **19**, 827 (2018).
[25] A. Michel and B. Arcen, Long time statistics of prolate spheroids dynamics in a turbulent channel flow, Int. J. Multiphase Flow **135**, 103525 (2021).
[26] F. Picano, G. Sardina, and C. M. Casciola, Spatial development of particle-laden turbulent pipe flow, Phys. Fluids **21**, 093305 (2009).
[27] I. Gallily and A.-H. Cohen, On the orderly nature of the motion of nonspherical aerosol particles. II. Inertial collision between a spherical large droplet and an axially symmetrical elongated particle, J. Colloid Interface Sci. **68**, 338 (1979).
[28] Y. Cui, J. Ravnik, M. Hriberšek, and P. Steinmann, A novel model for the lift force acting on a prolate spheroidal particle in an arbitrary non-uniform flow. Part I. Lift force due to the streamwise flow shear, Int. J. Multiphase Flow **104**, 103 (2018).

[29] C. Siewert, R. Kunnen, M. Meinke, and W. Schröder, Orientation statistics and settling velocity of ellipsoids in decaying turbulence, Atmos. Res. **142**, 45 (2014).
[30] M. Shapiro and M. Goldenberg, Deposition of glass fiber particles from turbulent air flow in a pipe, J. Aerosol Sci. **24**, 65 (1993).
[31] A. Oberbeck, Uber stationare flussigkeitsbewegungen mit beracksichtigung der inneren reibung, J. Reine Angew. Math. **81**, 62 (1876).
[32] A. W. Vreman and J. G. M. Kuerten, Comparison of direct numerical simulation databases of turbulent channel flow at $\mathrm{Re}_\tau = 180$, Phys. Fluids **26**, 015102 (2014).
[33] H. Le and P. Moin, An improvement of fractional step methods for the incompressible Navier-Stokes equations, J. Comput. Phys. **92**, 369 (1991).
[34] L. J. P. Timmermans, P. D. Minev, and F. N. van de Vosse, An approximate projection scheme for incompressible flow using spectral elements, Int. J. Numer. Methods Fluids **22**, 673 (1996).
[35] R. Moser, J. Kim, and N. Mansour, Direct numerical simulation of turbulent flow in a channel up to $\mathrm{Re}_\tau = 590$, Phys. Fluids **11**, 943 (1999).
[36] M. Lee and R. D. Moser, Direct numerical simulation of turbulent channel flow up to $Re_\tau \approx 5200$, J. Fluid Mech. **774**, 395 (2015).
[37] C. E. Shannon, A mathematical theory of communication, Bell Syst. Tech. J. **27**, 379 (1948).
[38] C. Marchioli and A. Soldati, Mechanisms for particle transfer and segregation in a turbulent boundary layer, J. Fluid Mech. **468**, 283 (2002).
[39] M. Bernardini, Reynolds number scaling of inertial particle statistics in turbulent channel flows, J. Fluid Mech. **758**, R1 (2014).
[40] M. Alipour, M. De Paoli, S. Ghaemi, and A. Soldati, Long non-axisymmetric fibres in turbulent channel flow, J. Fluid Mech. **916**, A3 (2021).
[41] M. Do-Quang, G. Amberg, G. Brethouwer, and A. V. Johansson, Simulation of finite-size fibers in turbulent channel flows, Phys. Rev. E **89**, 013006 (2014).
[42] P. Costa, L. Brandt, and F. Picano, Near-wall turbulence modulation by small inertial particles, J. Fluid Mech. **922**, A9 (2021).
[43] S. Shaik, S. Kuperman, V. Rinsky, and R. van Hout, Measurements of length effects on the dynamics of rigid fibers in a turbulent channel flow, Phys. Rev. Fluids **5**, 114309 (2020).
[44] L. Zhao and H. I. Andersson, Why spheroids orient preferentially in near-wall turbulence, J. Fluid Mech. **807**, 221 (2016).
[45] R. L. Panton, Scaling and correlation of vorticity fluctuations in turbulent channels, Phys. Fluids **21**, 115104 (2009).
[46] A. Pumir and M. Wilkinson, Orientation statistics of small particles in turbulence, New J. Phys. **13**, 093030 (2011).